

To: Public

Cc:

From: Will Levandowski, PhD
will.levandowski@tetrtech.com

Date: April 12, 2023

Subject: Hispaniola Stress Map and Fault Slip Potential Modeling

Introduction

This memorandum presents a preliminary investigation of the crustal stress field in Hispaniola and preliminary fault slip potential (FSP) models of the island. Crustal stress is determined by inversions of earthquake focal mechanisms (**Figure 1**) for the island as a whole and for several discrete regions. The resulting stress tensors are used as input for FSP models, which provide a quantitative measure of the suitability of faults for slip in the local stress field as a function of fault orientation.

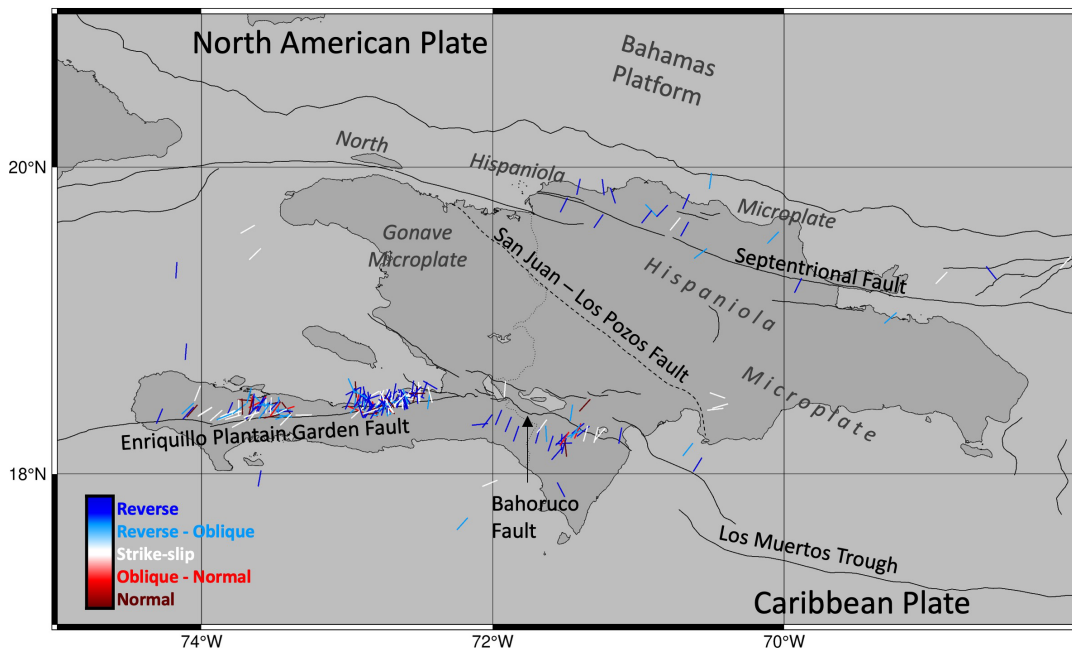


Figure 1: Regional tectonic elements. Microplates labeled in dark gray. Faults shown as black lines. Focal mechanisms used for stress inversions are shown as bars colored by faulting style and oriented in the horizontal maximum shortening direction for each event.

Hispaniola lies near the NE edge of the Caribbean plate, where it converges obliquely with and overrides the Atlantic oceanic lithosphere [Calais et al., 2016]. Collision of Hispaniola with the buoyant Bahamas Platform to the NNE generates additional compressional tractions and contractile structures offshore [e.g., Mann et al., 2002]. Substantial left-lateral deformation within Hispaniola partitions into two high strain-rate bands: the Enriquillo Plantain Garden Fault Zone (EPGF) along the southern edge and Septentrional Fault Zone (SFZ) along the northern edge, with relative quiescence between (**Figure 2**). Earthquakes concentrate along the high strain-rate EPGF and SFZ and also diffusely in easternmost Hispaniola (**Figure 3**).

This partitioning allows the region to be separated into three microplates separated from the Caribbean plate by major faults (**Figure 1**). The deforming North Hispaniola microplate lies north of the SFZ. The quiescent Hispaniola

microplate to the south covers central to southeastern Dominican Republic (DR) and the NE corner of Haiti, bounded on its southern side by the Los Muertos Trough and then the Caribbean plate. Finally, the Gonave microplate comprises most of Haiti and a small portion of SW Dominican Republic; the EPGF and Bahoruco Faults mark the boundary between the Gonave microplate and the Caribbean plate to the south. The boundary between the Gonave and Hispaniola microplates likely trends WNW across the island along the San Juan-Los Pozos thrust fault but is not clearly expressed (**Figure 1**).

Figure 2: Strain rates (from Calais et al., 2016)

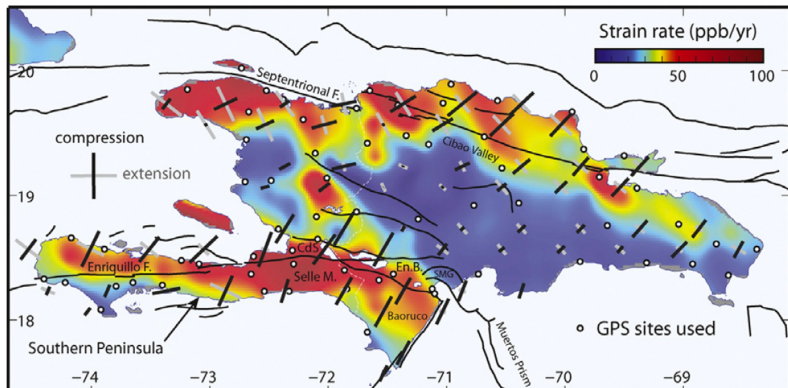


Figure 3: Seismicity $M \geq 3$ since 1974 from USGS/ANSS Comprehensive Catalog.

Crustal Stress

The crustal stress field is constrained with focal mechanisms from 226 crustal earthquakes, depths ≤ 30 km and averaging 9.8 km [USGS, 2023; Rodriguez et al., 2018; Douilly et al., 2013; 2022]. Most display reverse to strike-slip mechanisms with P-axes oriented NNE-SSW (**Figure 4a-b**). The World Stress Map [Heidbach et al., 2018] contains no in-situ measurements—such as borehole breakouts—for the island.

Some differences appear across the island. Many of the 170 events in Haiti are aftershocks of the 2010 and 2021 Haiti M7 earthquakes (on the Gonave microplate); the P-axes and faulting styles of these earthquakes (**Figure 4c-d**) vary more than events in the DR, likely reflecting the role of spatially and temporally varying stress transfer and post-seismic phenomena. Nevertheless, the 32 earthquakes from the southwestern DR and the SE corner of Haiti on the Gonave microplate (**Figure 4e-f**) have more variable mechanisms than the 21 from the North Hispaniola microplate (**Figure 4g-h**), perhaps because of interactions across the complex network of intersecting faults between the EPGF and Los Muertos Trough. Three events within the central Hispaniola microplate (**Figure 1**) have

consistent E–W P-axes and strike-slip mechanisms that may indicate a somewhat different deformation regime in that low-strain block.

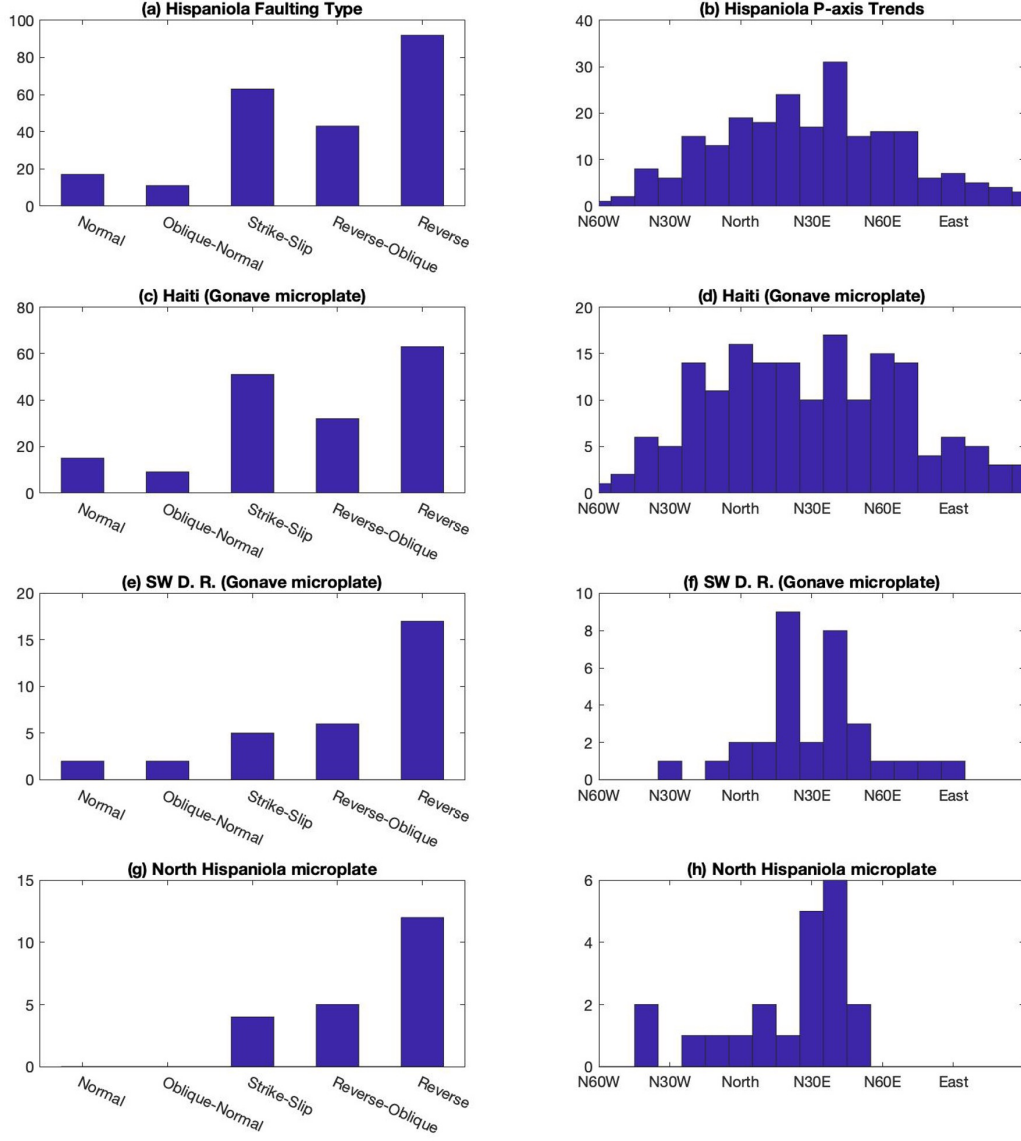


Figure 4: Focal mechanism parameters for the entire dataset (a-b) and for geographic subsets (c-h). Left column: faulting type. Right column: Horizontal shortening directions (P-axes for strike-slip to reverse faulting).

The focal mechanisms are next inverted to determine the best-fitting normalized stress tensor for the island as a whole, for the Haitian subset, the southwestern Dominican Republic within the Gonave microplate, and for North Hispaniola. Such inversions are well established and stem from the axiom that coseismic slip parallels the shear traction resolved on the fault plane [e.g., Angelier, 1979]. The latter depends linearly on the orientation of the fault and on the 3D stress tensor. Assuming that earthquakes in a small region are all responding to a similar 3D stress field, this linear system quickly becomes overdetermined with multiple slip observations

from faults of different orientations. By convention, about 20 focal mechanisms are needed for reliable stress inversions [e.g., Townend and Zoback, 2004]. Inverting this linear system solves for the 3D stress tensor that minimizes the angular misfit between the slip vectors and shear traction on the respective fault planes.

The normalized stress tensor can be fully described in terms of the directions and ratio of magnitudes of the principal stresses ϕ :

$$\phi = (S_2 - S_3) / (S_1 - S_3)$$

with S_1 the magnitude of the maximally compressive stress, S_2 intermediate, and S_3 the minimum.

Simpson [1997] combined ϕ with the style of faulting (normal/strike-slip/reverse, as defined by principal axis plunges [Zoback, 1992]) to describe the style of deformation as a quantity $A\Phi$:

$$A\Phi = (n + 0.5) + (-1)^n(\phi - 0.5)$$

with $n=0$ for normal faulting, 1 for strike-slip, and 2 for thrust.

Consequently, $A\Phi$ defines a continuum from radial extension ($A\Phi = 0$) to radial contraction ($A\Phi = 3$), passing through: uniaxial extension/pure normal faulting ($A\Phi=0.5$); oblique extension ($A\Phi=1.0$); horizontal shear/strike-slip ($A\Phi=1.5$); oblique contraction ($A\Phi=2.0$), and uniaxial contraction/pure thrust, ($A\Phi=2.5$).

The inversion algorithm [following Levandowski et al., 2018a] appraises uncertainty with Monte Carlo realizations. Each realization begins by jackknife-resampling the dataset (discarding $n_{\text{mechanisms}}^{0.5}$), randomly perturbing the individual slip vectors by $\pm 15^\circ$, and choosing a random coefficient of friction between 0.4 and 0.9. The retained mechanisms are then iteratively inverted [following Vavryčuk, 2014], selecting the less stable of the two nodal planes for each event with respect to the current estimate of the stress tensor, inverting these mechanisms for an updated stress estimate, and recomputing the stability of each plane, for a total of 5 iterations per realization. A total of 100 realizations are used for each inversion, and the values discussed are the median \pm one standard deviation.

Fault Slip Potential Modeling

FSP modeling provides a quantitative metric for how well faults are oriented for frictional slip in the local stress field. From the estimate of the normalized stress tensor derived from focal mechanisms, the full stress tensor is calculated [following Walsh and Zoback, 2016; Levandowski et al., 2018b] at a nominal depth, here 10 km. The shear and normal tractions on a fault plane of any orientation can be readily computed from the full stress tensor, and the suitability of faults is then quantified in terms of distance from Coulomb failure, or the difference between the computed shear traction magnitude and the critical shear traction:

$$dCFS = \text{friction} \times |\text{effective normal traction}| - |\text{shear traction}|$$

Thus, dCFS represents the shear stress increase that may trigger slip on a pre-existing fault. The underlying assumption of FSP modeling is that the crust is in a state of frictional failure equilibrium [e.g., Zoback, 2010], meaning that a fault with the optimal orientation in the local stress field has $dCFS = 0$ MPa. Alternatively, FSP can be quantified in terms of the pore fluid pressure increase ΔP required to trigger slip. The optimal fault orientation has $\Delta P=0$, while faults that remain stable with total pore pressure equal to S_3 are incompatible with frictional slip, as hydrofracture would occur before shear traction overcomes frictional resistance.

Results

Across Hispaniola, NNE-SSW horizontal shortening dominates. Inversion of the full dataset (**Figure 5**) yields best-fitting maximum horizontal compression $\sigma_{H\max}$ N28E $\pm 1^\circ$ and $A\Phi=2.14\pm 0.02$. Consequently, FSP models

indicate that gently dipping, $\sim 30^\circ$, ESE- and WSW-striking faults have the greatest tendency for slip (**Figure 6a**). Moderately high slip potential (low dCFS) defines continua from near-vertical NE-striking (strike-slip) faults through the gently dipping ESE-striking optimal (reverse) fault orientation back to near-vertical S-striking (strike-slip) faults and along diametric orientations. That is, NE-, S-, SW-, and N-striking faults may be active as strike-slip structures, in addition to the optimally oriented ESE- and WNW-striking reverse faults.

Since events in Haiti dominate the full Hispaniola dataset, it is not surprising that stress inversions and FSP models for the Haitian data are indistinguishable from the island-wide results (**Figure 5b**)

The North Hispaniola subset, the smallest, produces insignificantly different results from the island-wide modeling: $\sigma_{H\max}$ N34E $\pm 5^\circ$ and $A\phi=2.22\pm 0.08$ (**Figure 5**). Again, gently dipping, ESE- or WNE-striking reverse faults are the best oriented, with slip also possible on NE-SW or N-S strike-slip faults (**Figure 6c**).

The Gonave microplate portion of southwestern DR shares NNE $\sigma_{H\max}$ (N32E $\pm 4^\circ$) with the rest of the island but has a slightly less compressive stress field (**Figure 5**). With $A\phi=2.04\pm 0.08$, the vertical stress and the minimum horizontal stress have insignificantly different magnitudes, allowing an even mix of reverse and strike-slip faulting. Slip is equally possible on gently dipping, ESE- or WNE-striking reverse faults and on NE-SW or N-S strike-slip faults (**Figure 6d**).

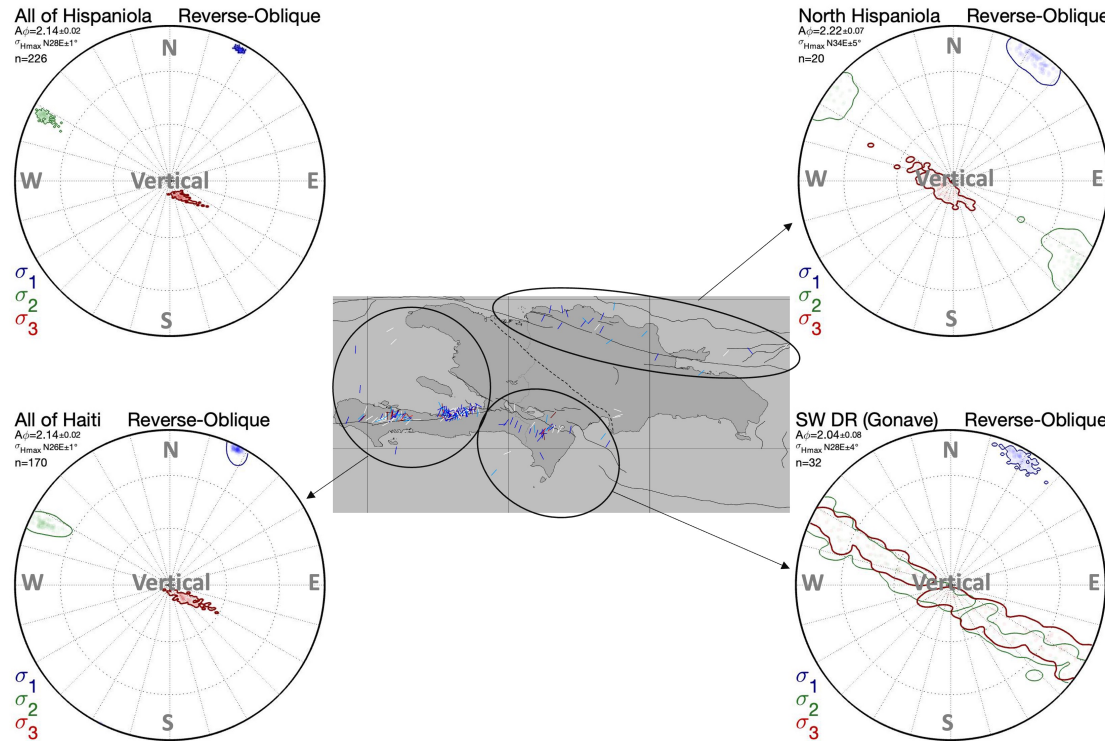


Figure 5: Stress inversion results for the full dataset (top left) and geographic subsets. No statistically significant differences are found across the island.

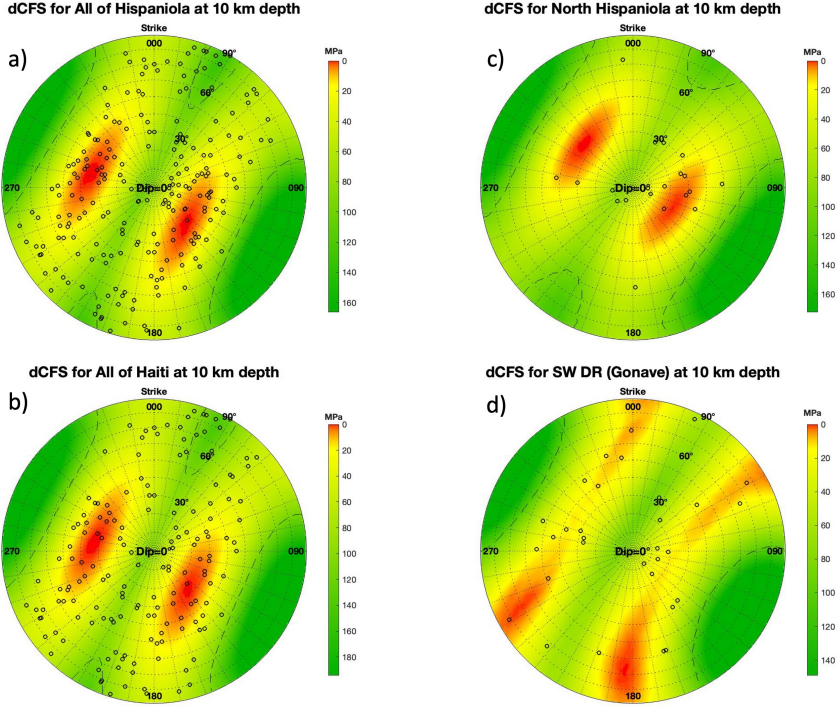


Figure 6: Fault slip potential modeling for the full dataset (top left) and geographic subsets. Haiti and North Hispaniola favor reverse faulting on gently dipping planes striking SE and NW, while SW DR favors oblique contraction on more steeply dipping, N–S and NE–SW faults. Circles indicate the strike and dip of the preferred nodal plane for each focal mechanism used in the modeling. Dashed line: Hydrofracture gradient. Note that all faults dipping more than ~60° and striking in the SE or NW quadrant lie beyond the hydrofracture gradient, meaning they are incapable of frictional slip.

Conclusions

The crustal stress field across Hispaniola is characterized by NNE–SSW maximal compression and favors reverse to strike-slip faulting. Statistically insignificant differences from the North Hispaniola microplate to the portion of the Gonave microplate in SW DR and into Haiti suggest slightly more contraction along the SFZ than the Bahoruco Fault or EPGF. Several fault orientations are well oriented for slip in the modern stress field (**Figure 7**). Gently dipping, ~30°, planes striking generally ESE or WNW are optimally aligned for reactivation as thrust faults. Near-vertical faults oriented N–S or ENE–WSW are prone to reactivation as strike-slip faults. By contrast, planes dipping more than ~60° and striking anywhere in the SE or NW quadrants are unlikely to slip and may be frictionally locked.

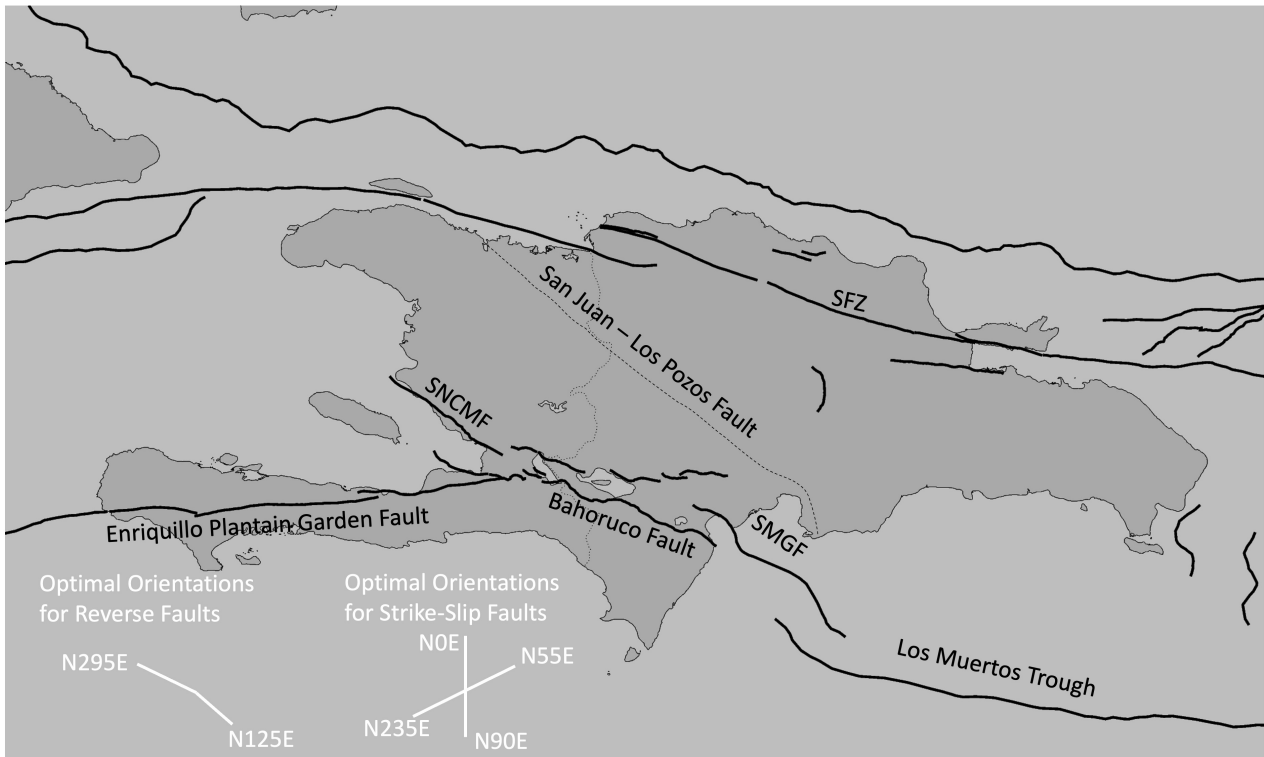


Figure 7: Optimal fault orientations and mapped faults for comparison. Reverse faults striking WNW, such as the Septentrional Fault Zone, are well aligned for slip in the modern stress field. Steep ENE-WSW faults such as the Enriquillo Plantain Garden Fault are well oriented for strike-slip. Although steep N–S faults are also well aligned, there are few faults of this orientation.

References

- Angelier, J. (1979) Determination of the mean principal stresses for a given fault population, *Tectonophysics* 56, T17-T26, 1979.
- Angelier, J., Inversion of field data in fault tectonics to obtain the regional stress, III, A new rapid direct inversion method by analytical means, *GeophysJ. . Int.*, 103, 363-376, 1990.
- Calais E, Symithe S, Mercier de Lepinay B, Prepetit C (2016) Plate boundary segmentation in the northeastern Caribbean from geodetic measurements and Neogene geological observations. *Compt Rendus Geosci* 348:42–51
- Douilly R, Haase JS, Ellsworth WL, Bouin M, Calais E, Symithe SJ, Armbruster JG, Lépinay BM, Deschamps A, Mildor S, Meremonte ME, Hough SE (2013) Crustal structure and fault geometry of the 2010 Haiti earthquake from temporary seismometer deployments. *Bull Seismol Soc Am* 103:2305–2325
- Douilly, R., Paul, S., Monfret, T., Deschamps, A., Ambrois, D., Symithe, S. J., ... & Chèze, J. (2023). Rupture segmentation of the 14 August 2021 M w 7.2 Nippes, Haiti, earthquake using aftershock relocation from a local seismic deployment. *Bulletin of the Seismological Society of America*, 113(1), 58-72
- Heidbach, O., M. Rajabi, X. Cui, K. Fuchs, B. Müller, J. Reinecker, K. Reiter, M. Tingay, F. Wenzel, F. Xie, M. O. Ziegler, M.-L. Zoback, and M. D. Zoback (2018): The World Stress Map database release 2016: Crustal stress pattern across scales. *Tectonophysics*, 744, 484-498, doi:10.1016/j.tecto.2018.07.007
- Heidbach, Oliver; Rajabi, Mojtaba; Reiter, Karsten; Ziegler, Moritz, WSM Team (2016): World Stress Map Database Release 2016. GFZ Data Services, doi:10.5880/WSM.2016.00

- Levandowski, W., Weingarten, M., and Walsh F.R. III. (2018) Geomechanical sensitivities of injection-induced earthquakes: *Geophysical Research Letters*, v. 45, doi:10.1029/2018GL077551
- Levandowski, W., Herrmann, R.B., Briggs, R., Boyd, O.S., and Gold, R. (2018) A revised stress map of the continental United States reveals evidence for heterogeneous intraplate stress: *Nature Geoscience*, v. 11, doi:10.1038/s41561-018-0120-x.
- Mann, P., Calais, E., Ruegg, J.-C., DeMets, C., Jansma, P.E., Mattioli, G.S., 2002. Oblique collision in the northeastern Caribbean from GPS measurements and geological observations. *Tectonics* 21 (6), 71726.
- Rodriguez, J., Havskov, J., Sørensen, M. B., & Santos, L. F. (2018). Seismotectonics of south-west Dominican Republic using recent data. *Journal of Seismology*, 22, 883-896.
- Simpson, R.W. (1997) Quantifying Anderson's faulting types. *BSSA* 102(B8).
- Townend, J., & Zoback, M. D. (2004). Regional tectonic stress near the San Andreas fault in central and southern California. *Geophysical Research Letters*, 31(15).
- Varryčuk, V. Iterative joint inversion for stress and fault orientations from focal mechanisms. *Geophys. J. Int.* 199, 69–77 (2014).
- Walsh, F. R. III, & Zoback, M. D. (2016). Probabilistic assessment of potential fault slip related to injection-induced earthquakes: Application to north-central Oklahoma, USA. *Geology*, 44(12), 991–994.
<https://doi.org/10.1130/G38275.1>
- Zoback, M. D. (2010). Reservoir geomechanics. New York: Cambridge University Press.
- Zoback, M.L., First and second-order patterns of stress in the lithosphere: The world stress map project, *Jour. Geophys Res.*, 97, 11,703-11,728, 1992.
-